Supplementary Table S1. ATM alterations in the 1,661-patient MSK-TMB study

Cancer Type	Total	Mutation	Fusion
Bladder Cancer	215	23	0
Colorectal Cancer	110	11	0
Melanoma	320	26	0
Cancer of Unknown Primary	88	7	0
Non-Small Cell Lung Cancer	350	23	0
Esophagogastric Carcinoma	126	6	1
Breast Cancer	44	2	0
Glioma	117	3	0
Renal Cell Carcinoma	151	2	0
Head and Neck Cancer	139	1	0

Supplementary Table S2. ATM alternations in the 10,945-patient MSK-IMPACT study

Cancer Type	Total	Mutation	Deep deletion	Amplification	Multi-alterations	Fusion
Small Bowl Cancer	35	7	0	0	0	0
Skin Cancer, Non-Melaoma	148	19	1	0	0	0
Bladder Cancer	423	45	2	0	0	0
Endometrial Cancer	218	24	0	0	0	0
Hepatobiliary Cancer	355	27	0	0	0	0
Colorectal Cancer	1007	75	0	0	0	1
Mature B-Cell Neoplasms	134	8	0	0	2	0
Non-Small Cell Lung Cancer	1668	120	0	2	1	0
Melanoma	365	23	0	0	0	0
Appendiceal Cancer	79	4	0	0	0	0
Small Cell Lung Cancer	82	4	0	0	0	0
Prostate Cancer	717	25	7	1	0	0
Histiocytosis	22	1	0	0	0	0
Salivary Gland Cancer	114	5	0	0	0	0
Thyroid Cancer	231	10	0	0	0	0
Cancer of Unknown Primary	186	8	0	0	0	0
Breast Cancer	1324	48	3	2	0	0
Adrenocortical Carcinoma	25	1	0	0	0	0
Mature T and NK Neoplasms	29	1	0	0	0	0
Renal Cell Carcinoma	361	12	0	0	0	0
Head and Neck Cancer	186	14	0	0	0	1
Pancreatic Cancer	502	69	7	2	0	0
Glioma	553	14	1	0	0	0
Soft Tissue Sarcoma	443	13	1	0	0	0
Esophagogastric Cancer	341	8	1	0	0	0
Peripheral Nervous System	80	0	2	0	0	0
Germ Cell Tumor	288	2	0	1	0	1
Ovarian Can	244	2	1	0	0	0
Uterine Sarcoma	93	1	0	0	0	0
Mesothelioma	107	1	0	0	0	0
Bone Cancer	134	1	0	0	0	0
Gastrointestinal Stromal Ca	137	0	0	0	0	1

Supplementary Table S3. SgRNA used in CRISPR/Cas9-mediated gene knockouts

Target	Sequence
Human-ATM-sg1	TTGTTTCAGGATCTCGAATC
Human-ATM-sg2	GATGCAGGAAATCAGTAGTT
Mouse-ATM-sg1	CTCTGTCATGCTCTAACTGC
Mouse-ATM-sg2	CTGTTTCAGGATCCTGAATC
Mouse-TFAM-sg1	ACGGGGGTCGAGATGTGCGC
Mouse-TFAM-sg2	TACCAGCGTGGGAACTCCGG
Mouse-cGAS	CAGAATGCAGAAACGGGAGT
Mouse-TBK	TGCCGTTTAGACCCTTCGAG
Mouse-Sting	CTTCTCGCTACAACACATGA
Mouse-MDA5	GGCAGGGATTCAGGCACCAT

Supplementary Table S4. Oligonucleotide primers for qPCR

Target	Sequence
Mouse-β-actin (F)	GAAATCGTGCGTGACATCAAA
Mouse-β-actin (R)	TGTAGTTTCATGGATGCCACA
Mouse-IFNβ1 (F)	CTGGCTTCCATCATGAACAA
Mouse-IFNβ1 (R)	AGAGGGCTGTGGTGGAGAA
Mouse-IFNα (F)	GGATGTGACCTTCCTCAGACTC
Mouse-IFNα (R)	ACCTTCTCCTGCGGGAATCCAA
Mouse-CCL5 (F)	CAAGTGCTCCAATCTTGCAGTC
Mouse-CCL5 (R)	TTCTCTGGGTTGGCACACAC
Mouse-IFIT1 (F)	CAAGGCAGGTTTCTGAGGAG
Mouse-IFIT1 (R)	GACCTGGTCACCATCAGCAT
Mouse-ISG15 (F)	CTAGAGCTAGAGCCTGCAG
Mouse-ISG15 (R)	AGTTAGTCACGGACACCAG
Mouse-mtDNA Dloop1 (F)	AATCTACCATCCTCCGTGAAACC
Mouse-mtDNA Dloop1 (R)	TCAGTTTAGCTACCCCCAAGTTTAA
Mouse-mtDNA Dloop2 (F)	CCCTTCCCCATTTGGTCT
Mouse-mtDNA Dloop2 (R)	TGGTTTCACGGAGGATGG
Mouse-mtDNA Dloop3 (F)	TCCTCCGTGAAACCAACAA
Mouse-mtDNA Dloop3 (R)	AGCGAGAAGAGGGGCATT
Mouse-mtDNA CytB (F)	GCTTTCCACTTCATCTTACCATTTA
Mouse-mtDNA CytB (R)	TGTTGGGTTGTTTGATCCTG
Mouse-mtDNA 16S (F)	CACTGCCTGCCCAGTGA
Mouse-mtDNA 16S (R)	ATACCGCGGCCGTTAAA
Mouse-mtDNA ND1(F)	CTAGCAGAAACAAACCGGGC
Mouse-mtDNA ND1 (R)	CCGGCTGCGTATTCTACGTT
Mouse-mtDNA ND4 (F)	AACGGATCCACAGCCGTA
Mouse-mtDNA ND4 (R)	AGTCCTCGGGCCATGATT
Mouse-mtDNA-Cox1 (F)	GCCCCAGATATAGCATTCCC
Mouse-mtDNA-Cox1 (R)	GTTCATCCTGTTCCTGCTCC
Mouse-nucDNA HK2 (F)	GCCAGCCTCTCCTGATTTTAGTGT

Mouse-nucDNA HK2 (R)	GGGAACACAAAAGACCTCTTCTGG
Mouse-nucDNA Tert (F)	CTAGCTCATGTGTCAAGACCCTCTT
Mouse-nucDNA Tert (R)	GCCAGCACGTTTCTCTCGTT
Mouse-nucDNA PTGER2 (F)	CCTGCTGCTTATCGTGGCTG
Mouse-nucDNA PTGER2 (R)	GCCAGGAGAATGAGGTGGTC
Mouse-nucDNA NDUFV1 (F)	CTTCCCCACTGGCCTCAAG
Mouse-nucDNA NDUFV1 (R)	CCAAAACCCAGTGATCCAGC

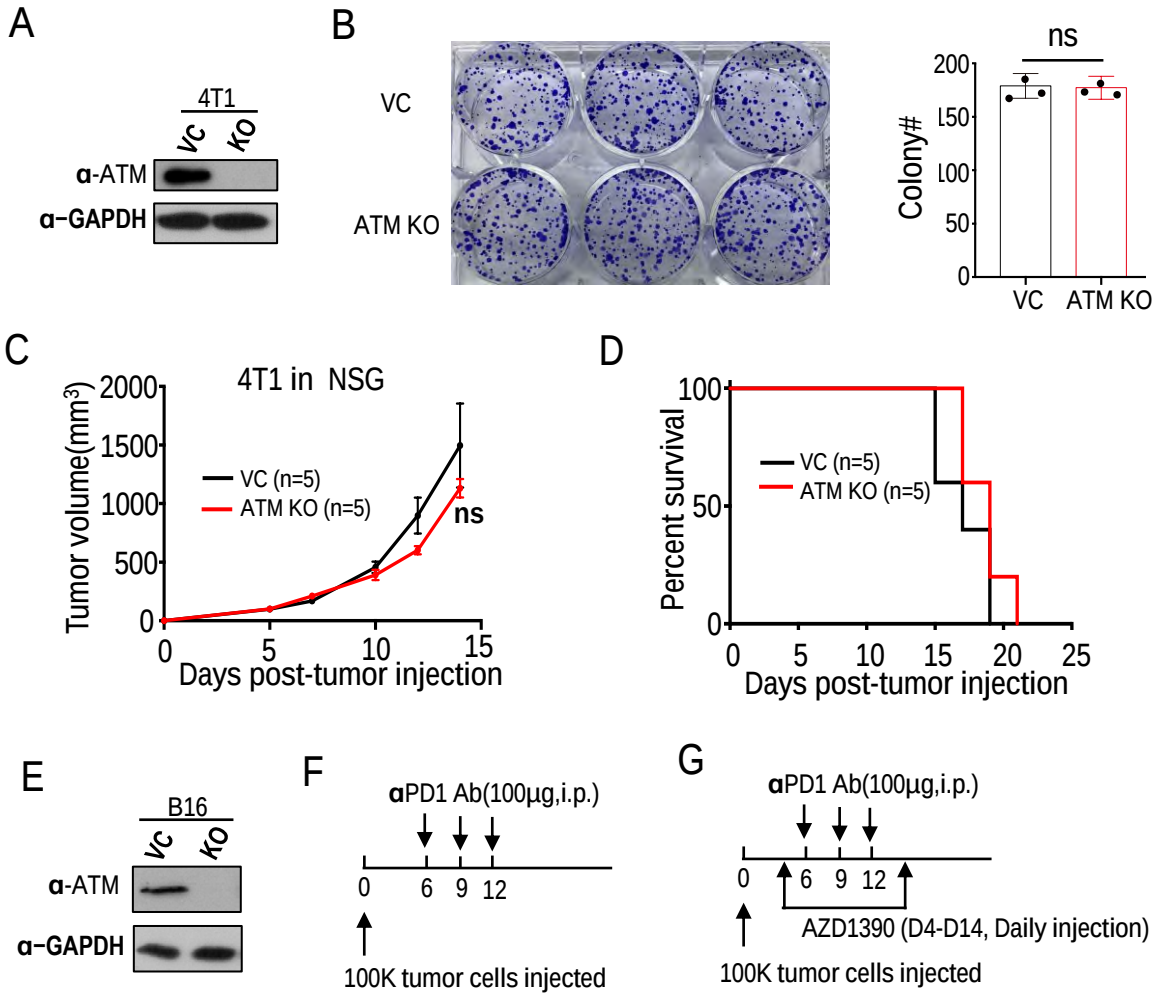

Supplementary Figure 1. ATM knockout and its effect on tumor growth in vitro and in vivo. (A) Western blot analysis of ATM expression in control and ATMKO 4T1 tumor cells . (B) Clonogenic abilities of vector control and ATM KO 4T1 cells. Cell were seeded in 6-well plates at 500 cells per well in triplicates and allowed to grow for 6 days before staining with crystal violet (left panel). The colony number were counted by use of Image J and plotted (right panel). (C-D) Tumor volume (C) and Kaplan-Meier survival curve (D) of immunodeficient NSG mice inoculated with about $1x10^5$ control or ATMKO 4T1 cells. (E) Western Blot analysis of ATM expression of vector control and ATMKO murine B16F10 tumor cells. (F) Treatment schedule for tumor growth delay experiments in Fig.1E, 1F. (G) Treatment schedule of tumor growth delay experiments in Fig.1G, 1H, 1I, 1J. Error bars represent ±SEM. NS, not significant, as determined by unpaired Student's t test (B and C) or log-rank test (D).

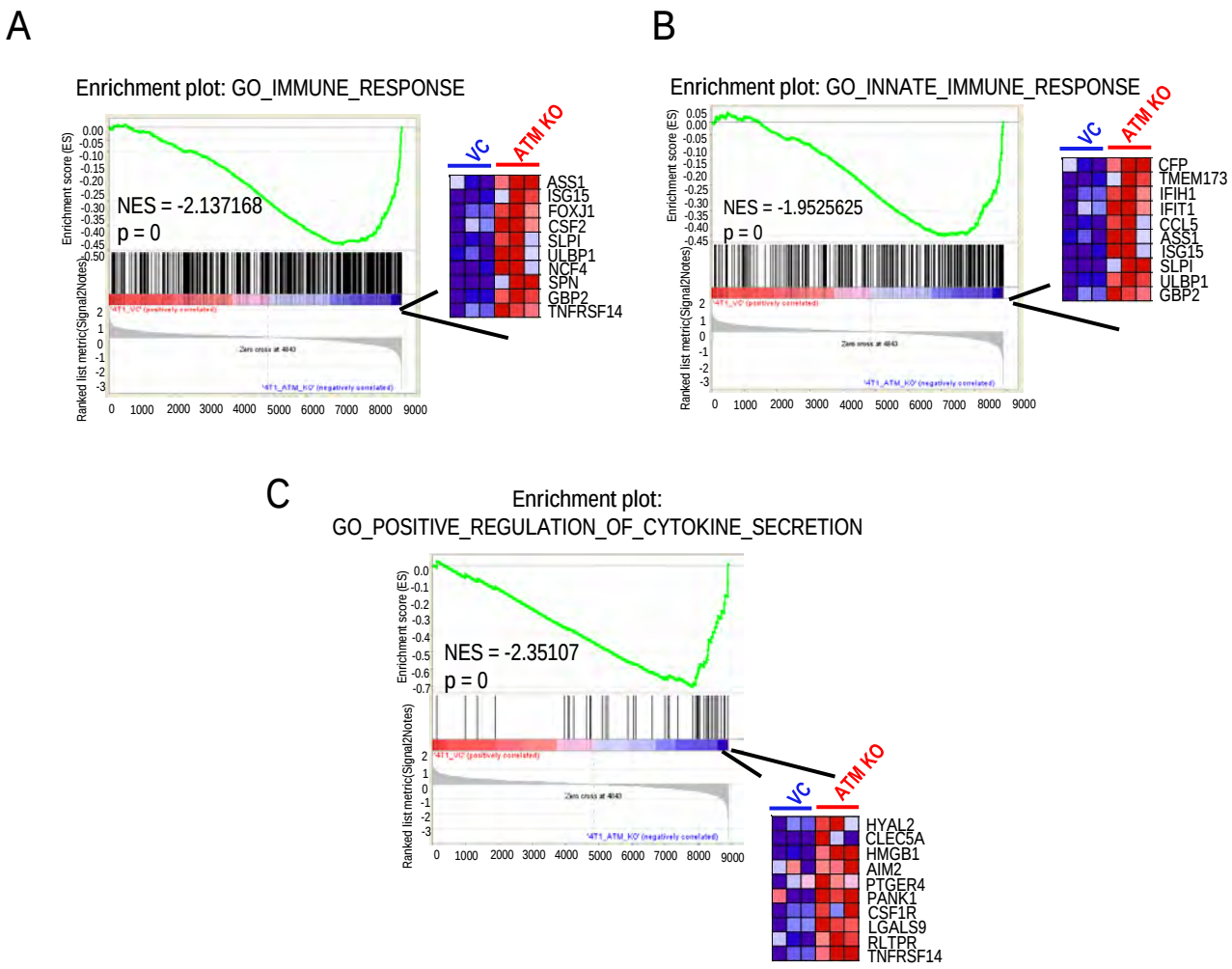

Supplementary Figure 2. Upregulation of expression of genes involved in innate immune response and cytokine secretion in ATM-deficient 4T1 cells in vitro. Gene set enrichment analysis (GSEA) of genes in involved in immune response (A), innate immune response (B), and cytokine secretion (C) in vector control and ATMKO 4T1 cells. FDR calculated using GSEA.

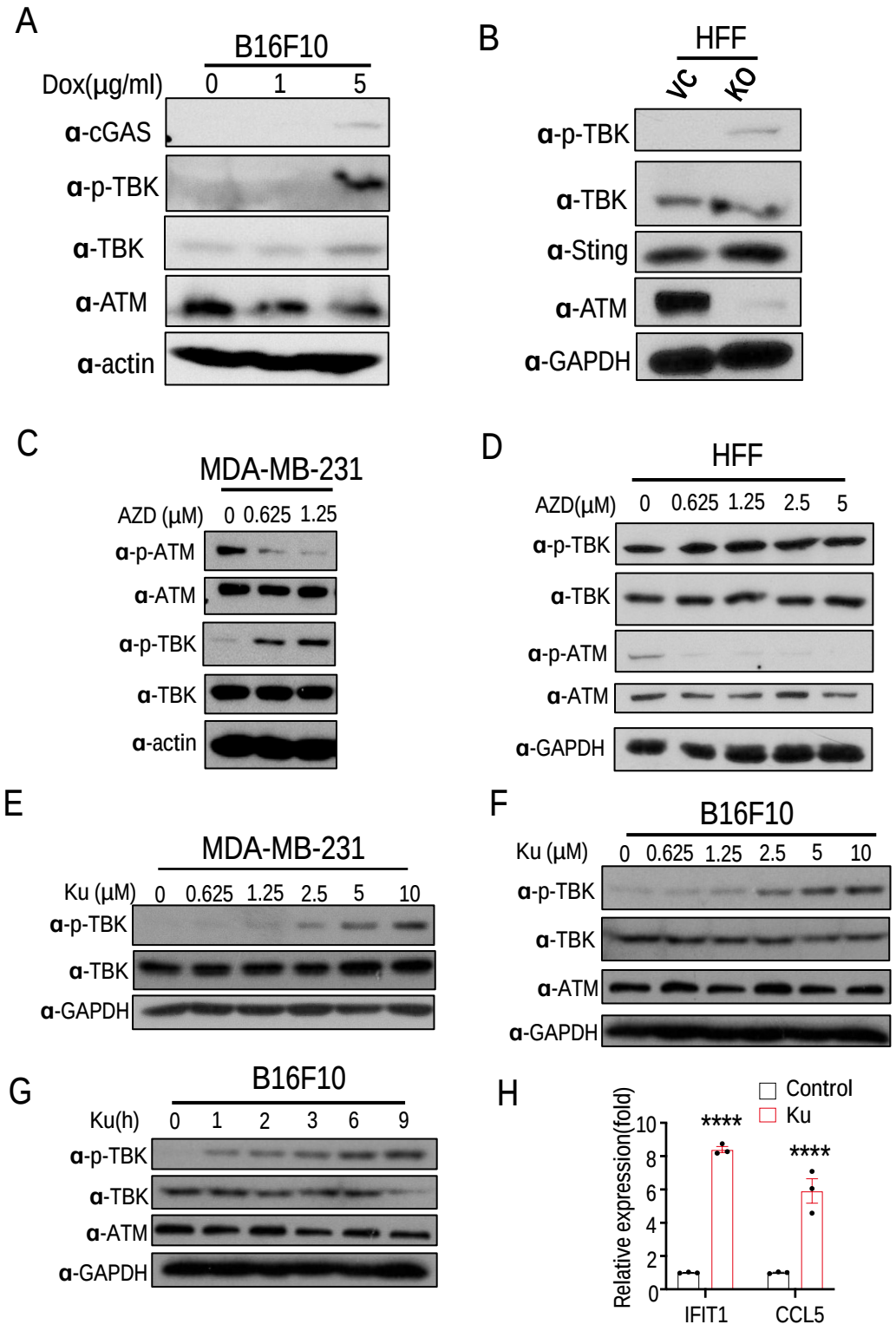

Supplementary Figure 3. Additional data on ATM inhibition induced cGAS-STING activation in malignant and normal cells. (A) WB analysis of p-TBK, TBK, cGas and ATM in B16F10 cells that had been transfected with inducible ATM shRNA and treated with doxycycline at indicated concentrations for 4 days. (B) WB analysis of p-TBK, TBK, STING and ATM in vector control(VC) and ATM KO human forskin fibroblast (HFF) cells. (C) WB analysis of p-ATM and p-TBK levels in MDA-MB-231 cells treated with AZD1390 at indicated concentrations for 48 hrs. (D) WB analysis of p-ATM and p-TBK levels in HFF cells treated with AZD1390 at indicated concentrations for 48 hrs. . (E) WB analysis of p-TBK and TBK in MDA-MB-231 cells treated with Ku55933 at indicated concentrations for 6 hrs. (F) WB analysis of p-TBK and TBK in B16F10 cells treated with 5 μM Ku55933 at indicated times. (G) WB analysis of p-TBK and TBK in B16F10 cells treated with Ku55933 (10 μM) for different times. (H) Transcription levels of IFIT1 and CCL5 in B16F10 cells treated with 10μM Ku55933 for 9 hrs and analyzed by real-time PCR. Error bars represent SEM, n=3, ***p<0.001, as determined by 2-way ANOVA

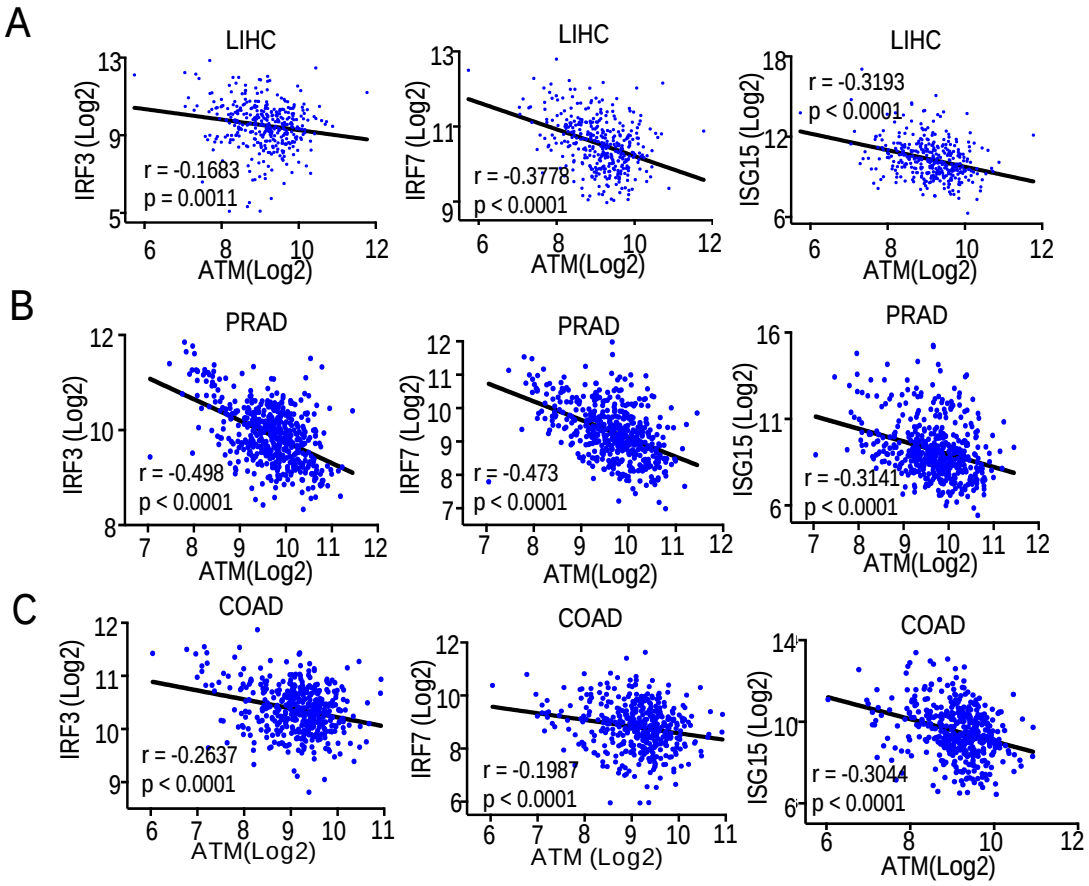

Supplementary Figure 4. Correlation between ATM and ISG gene transcriptional levels. Correlation analysis for ATM expression level versus IRF3, IRF7, and ISG15 in human (A) liver hepatocellular carcinoma (LIHC, 366 samples), (B) prostate adenocarcinoma (PRAD, 498 samples), (C) colorectal adenocarcinoma (COAD, 437 samples) from TCGA Pan Cancer Atlas. R and p represent Pearson correlation coefficients and p values from two-tailed Student's t-test.

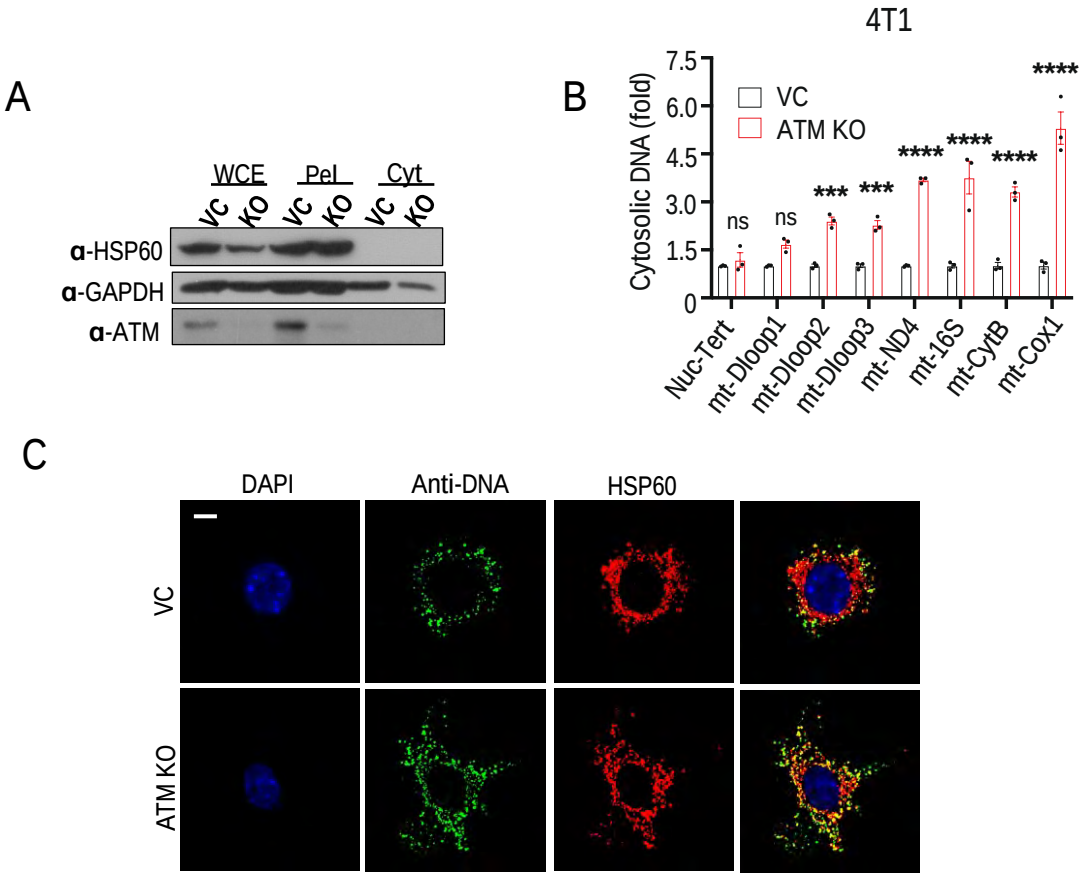

Supplementary Figure 5. Additional data validating mitochondrial DNA release as the key factor in ATM deficiency-mediated cGAS-STING activation. (A) WB analysis validating our cellular fractionation protocol. Vector control and ATM KO 4T1 cells were subjected to digitonin fractionation as described in the Methods. extracts (WCE), pellets (Pel) and cytosolic extracts(Cyt) were blotted using indicated antibodies. (B) DNA was extracted from digitonin extracts of vector control and ATM 4T1 cells. Cytosolic mtDNA was quantitated via qPCR using mitochondrial DNA primer sets and the nuclear gene TERT primer. Normalization was carried out as described in the Materials and Methods section. (C) Immunofluorescence detection of dsDNA location in vector control (VC) and ATM KO 4T1 cells by use of anti-dsDNA (green), anti-HSP60(red, for mitochondria), and DAPI (for nuclear DNA). Scale bar represents 10 μm. Error bars in B represent SEM, n=3, *p<0.05, **p<0.01, ***p<0.001, ****p<0.0001, ns, not significant, as determined by 2-way ANOVA.

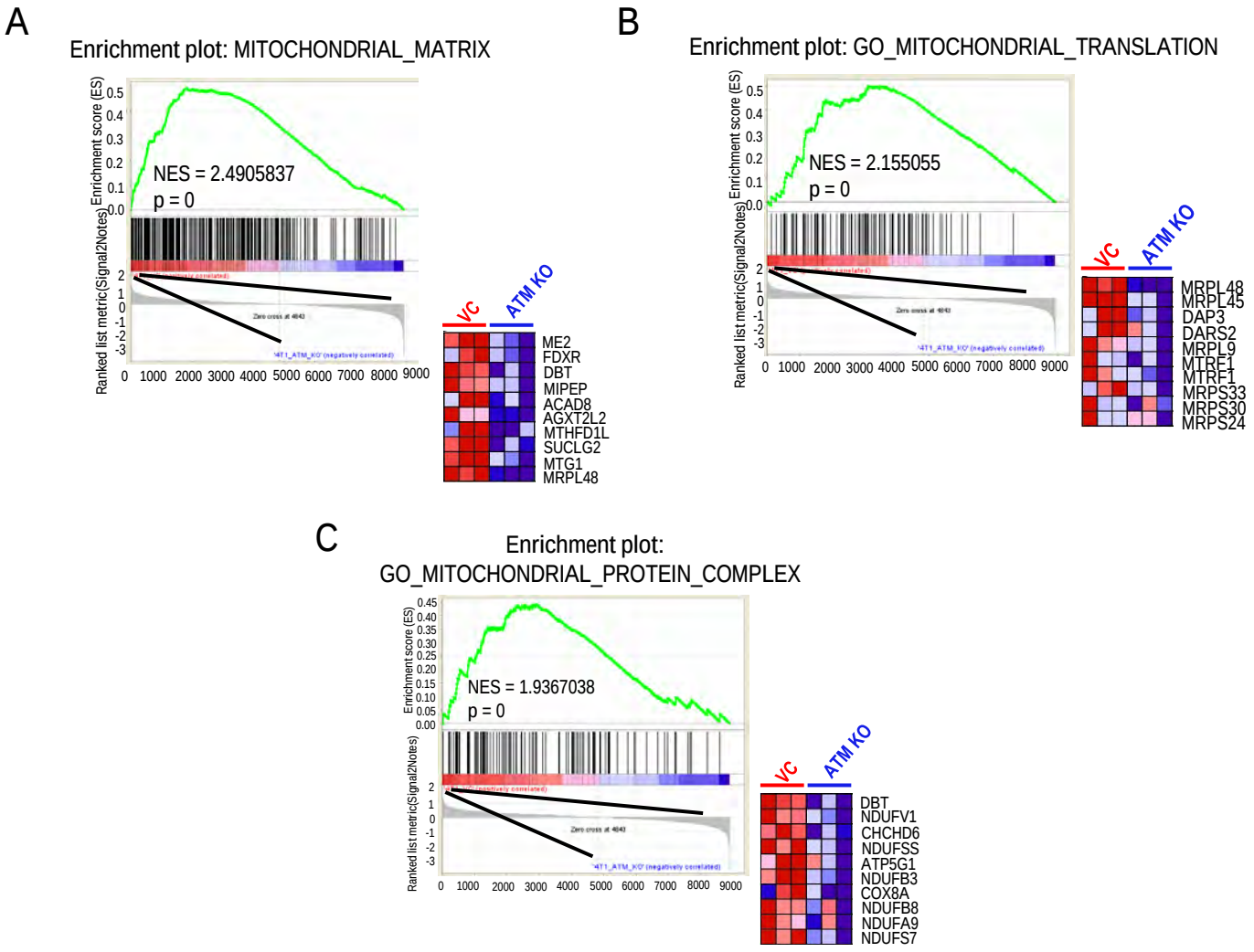

Supplementary Figure 6. Down-regulation of expression of genes involved in mitochondrial functions in ATM-deficient 4T1 cells in vitro. Gene set enrichment analysis (GSEA) of mitochondrial matrix genes (A), mitochondrial translation genes (B), and mitotochondrial protein complex genes (C) in control and ATM KO 4T1 tumor cells.

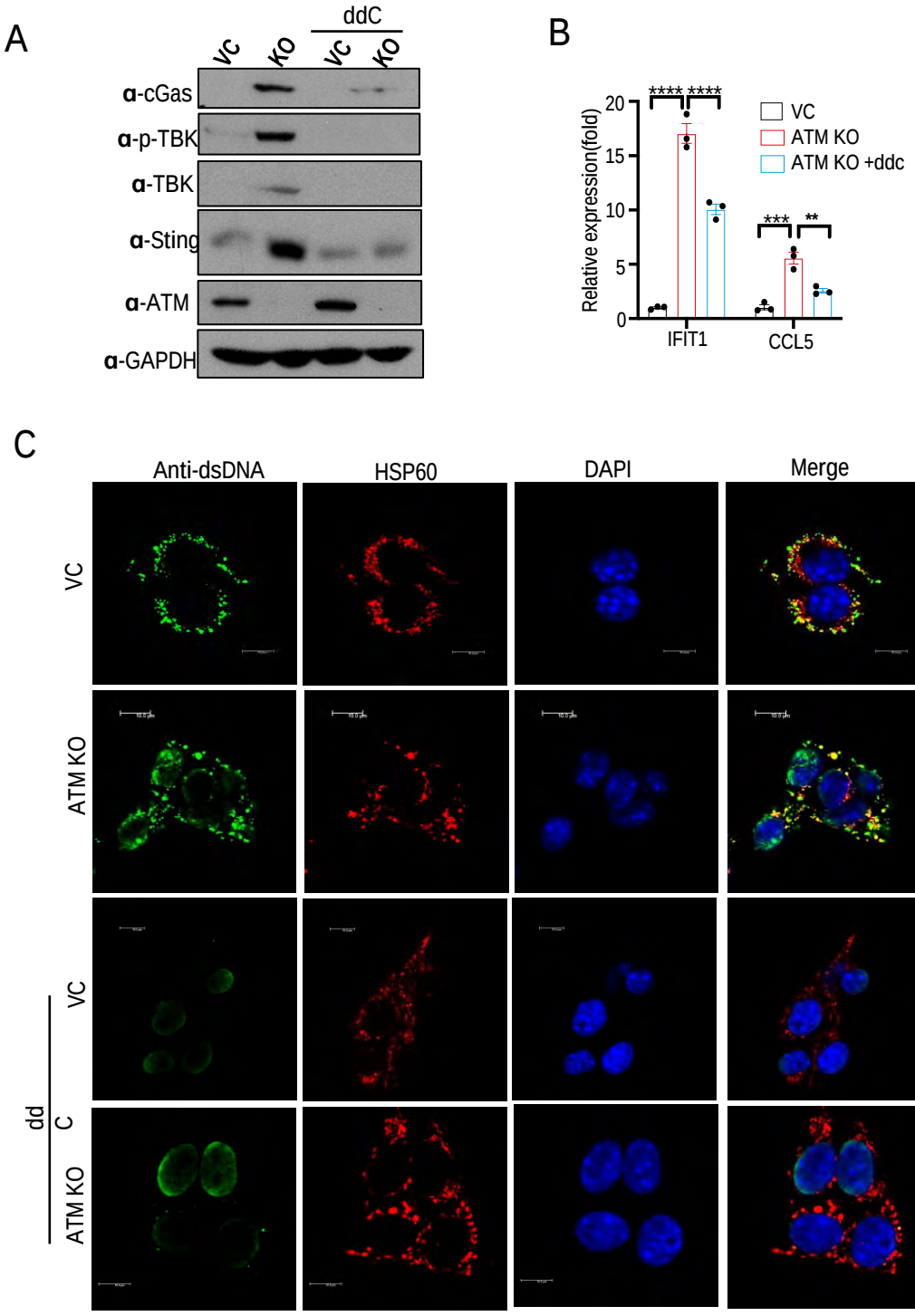

Supplementary Figure 7. Additional data validating cytoplasmic release of mtDNA being responsible for ATM inhibition induced cGAS-STING activation. (A) WB analysis of protein levels of pTBK, TBK, cGas and STING in control (VC) and ATM KO B16F10 cells exposed to 100 nM /ml ddC for 20 days to deplete mtDNA. (B) Q-PCR analysis of type I interferon response gene expression in vector control and ATMKO B16F10 cells that had been treated with 100 nM /ml ddC for 20 days to deplete mtDNA. (C) Control (VC) and ATM KO B16F10 cells that had been treated with 100 nM /ml ddC for 20 days were co-stained with anti-dsDNA (green), anti-HSP60(red) and DAPI. Scale bar indicated 10 μm. Error bars represent SEM, n=3, *p<0.05, **p<0.01, ***p<0.001, ****p<0.0001, ns, not significant, as determined by 2-way ANOVA.

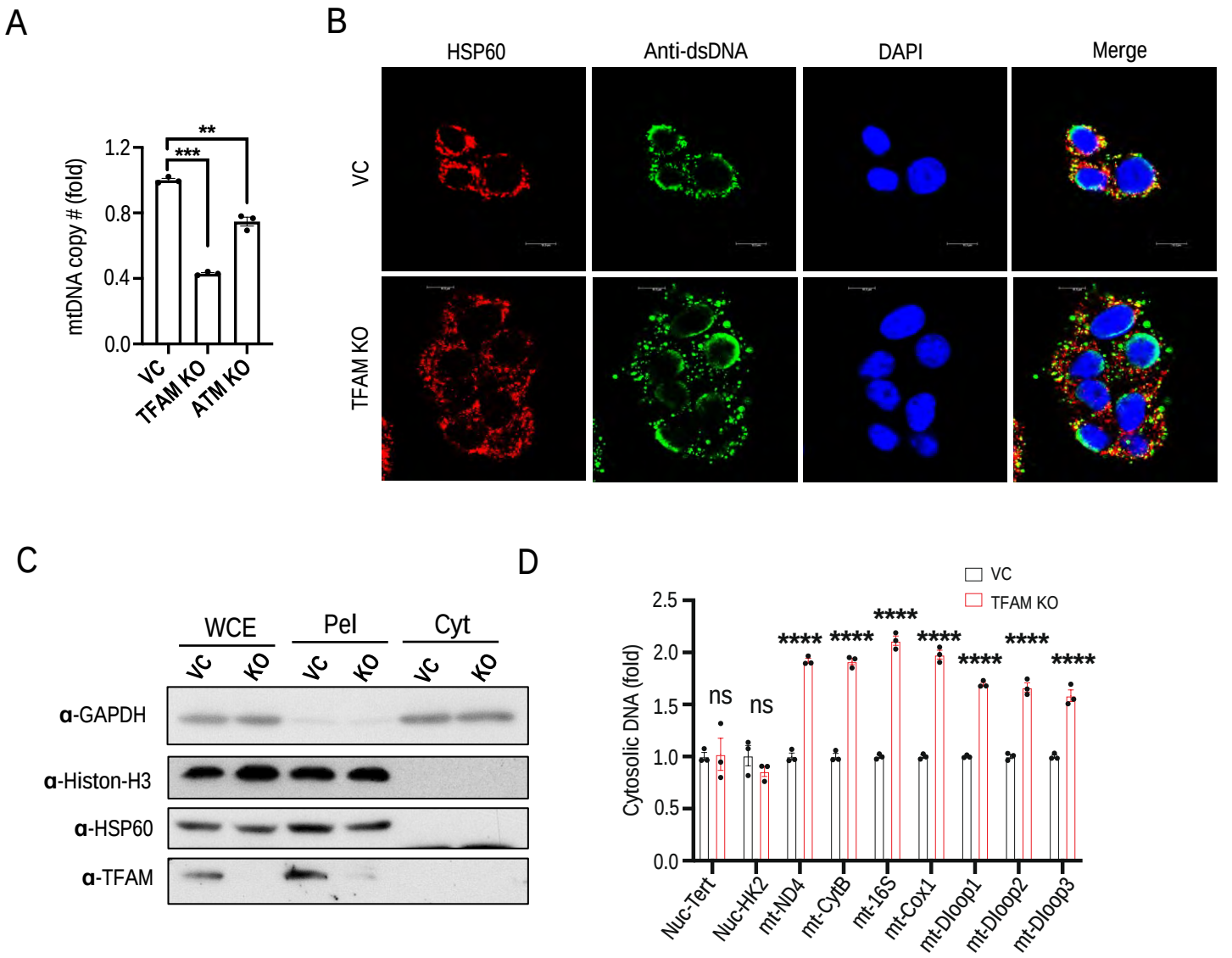

Supplementary Figure 8. Additional data validating mitochondrial DNA release as being involved in TFAM deficiency-mediated cGAS-STING activation. (A) qPCR analysis of mitochondrial copy number based on mitochondrial gene ND1 in vector control (VC) and TFAM KO or ATM KO B16F10 cells. (B) Immunofluorescence detection of dsDNA location in vector control (VC) and TFAM KO B16F10 cells by use of anti-dsDNA (green), anti-HSP60(red, for mitochondria), and DAPI (for nuclear DNA). Scale bar represents 10 μm. (C) WB analysis validating our cellular fractionation protocol. Vector control and TFAM KO B16F10 cells were subjected to digitonin fractionation as described in the Material and Methods section. Whole cell extracts (WCE), cell pellets (Pel) and cytosolic extracts(Cyt) were then blotted using indicated antibodies. (D) Cytosolic DNA was extracted from digitonin extracts of vector control and TFAM KO B16F10 cells. Cytosolic mtDNA was quantitated by qPCR using mitochondrial DNA primer sets and while nuclear DNA by use of the TERT gene primers. Normalization was carried out as described in the Materials and Methods section. Error bars in A & D represent SEM. *p<0.05, **p<0.01, ***p<0.001, ****p<0.0001 ns, not significant, as determined by 2-way ANOVA.

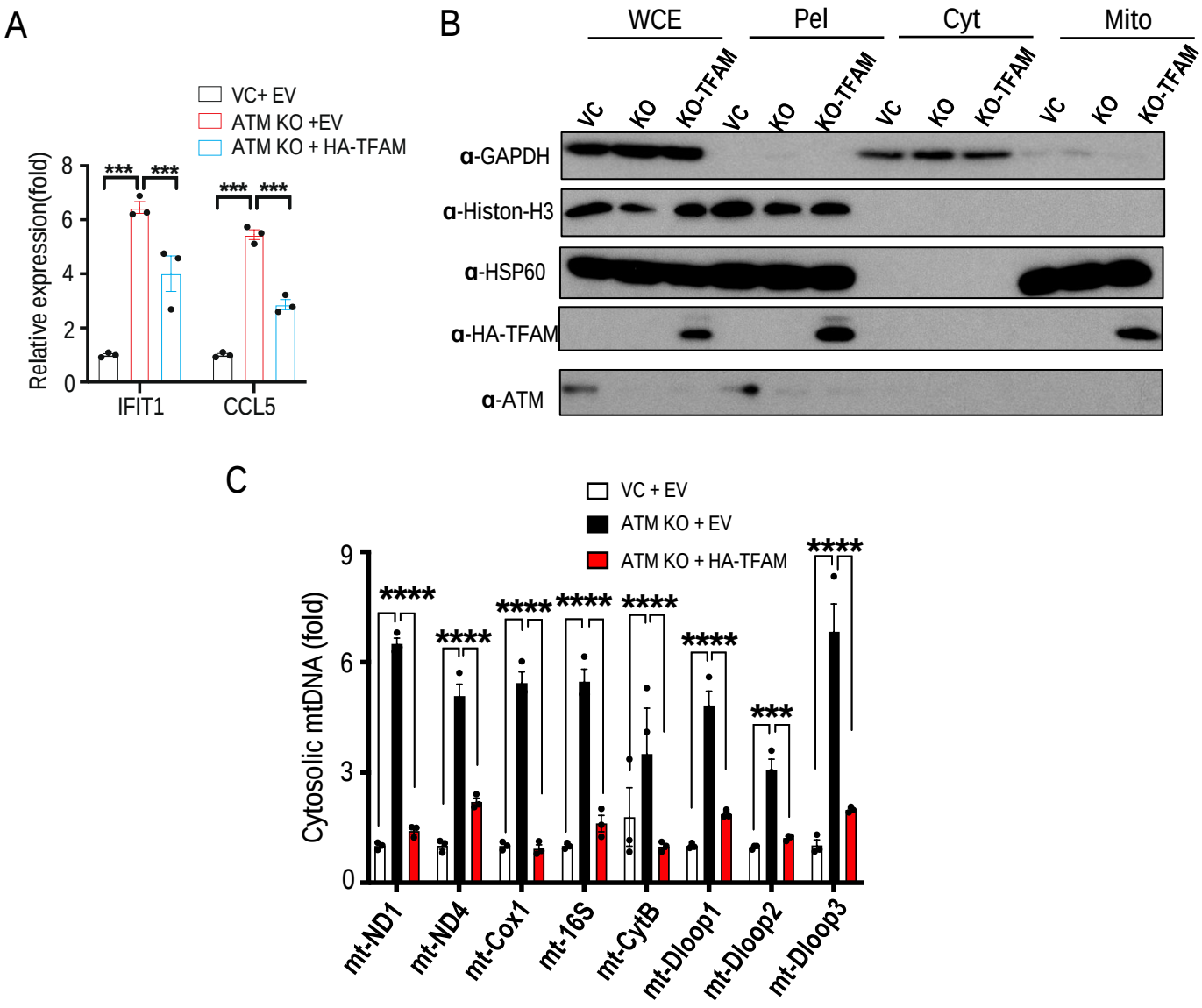

Supplementary Figure 9. Over-expression of TFAM in ATM KO cells inhibits release of mitochondria DNA and cGAS/STING activation. (A) Q-PCR analysis of interferon-stimulated gene expression in vector control and ATMKO B16F10 cells that had been transfected with empty vector (EV) or HA-TFAM. (B) WB verification of our cytosol fractionation protocol. Vector control and ATM KO B16 cells had been transfected with empty control (EV) or HA-TFAM were subjected to digitonin fractionation as described in the Methods and whole-cell extracts (WCE), pellets (Pel), cytosolic extracts(Cyt) and mitochondrion (Mito) were blotted using indicated antibodies. (C) Q-RT PCR quantification of cytosolic DNA extracted from digitonin-permeabilized cyotosolic extracts of control and ATM KO B16F10 cells that had been transfected with empty vector (EV) or HA-TFAM. Normalization was carried out as described in the Methods section. In A & C, error bars represent ±SEM, n=3, *p<0.05, **p<0.01, ***p<0.001, ****p<0.0001 ns, not significant, as determined by two-way ANOVA.

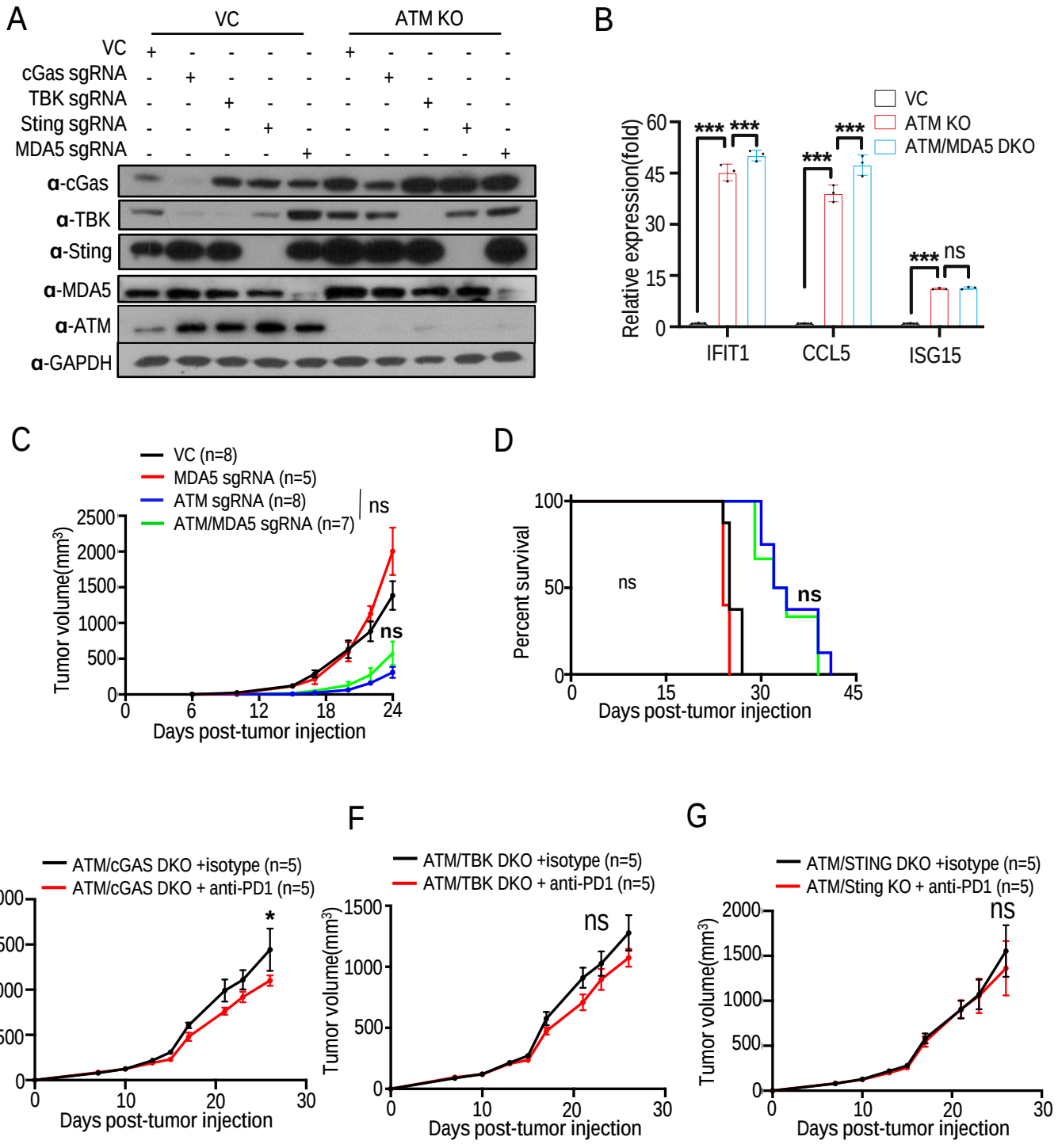

Supplementary Figure 10. MDA5 is not required for ATM deficiency mediates ISG activation and tumor growth delays. (A) WB verification of gene knockout for cGas, TBK, STING, and MDA5 in vector control (VC), and ATMKO cells. GAPDH was used as the protein loading control. (B) Transcriptional levels of interferon response genes in vector control (VC), ATM KO or or ATM/MDA5 DKO B16 cells analyzed by real-time qPCR. Error bars: SEM, n=3. ***p<0.001. (C-D) Tumor volume (C) and Kaplan-Meier survival curve (D) of C57BL/6 mice inoculated with $1x10^5$ vector control (VC), MDA5 KO, ATM KO, or ATM/MDA5 DKO B16F10 cells. The control groups VC and ATMKO are the same as shown in Fig. 6D-I. (E-G) Tumor growth in C57BL/6 mice inoculated with $1x10^5$ ATM KO or ATM/cGas DKO (E), ATM/TBK DKO (F), and ATM/STING DKO (G) B16F10 cells and treated with anti-PD1 antibody or isotype control (at 100μg/mouse) on days 6, 9, 12. Error bars represent SEM. *p<0.05, **p<0.01, ***p<0.001, ns, not significant, as determined by 2-way ANOVA (C) or log-rank test (D).

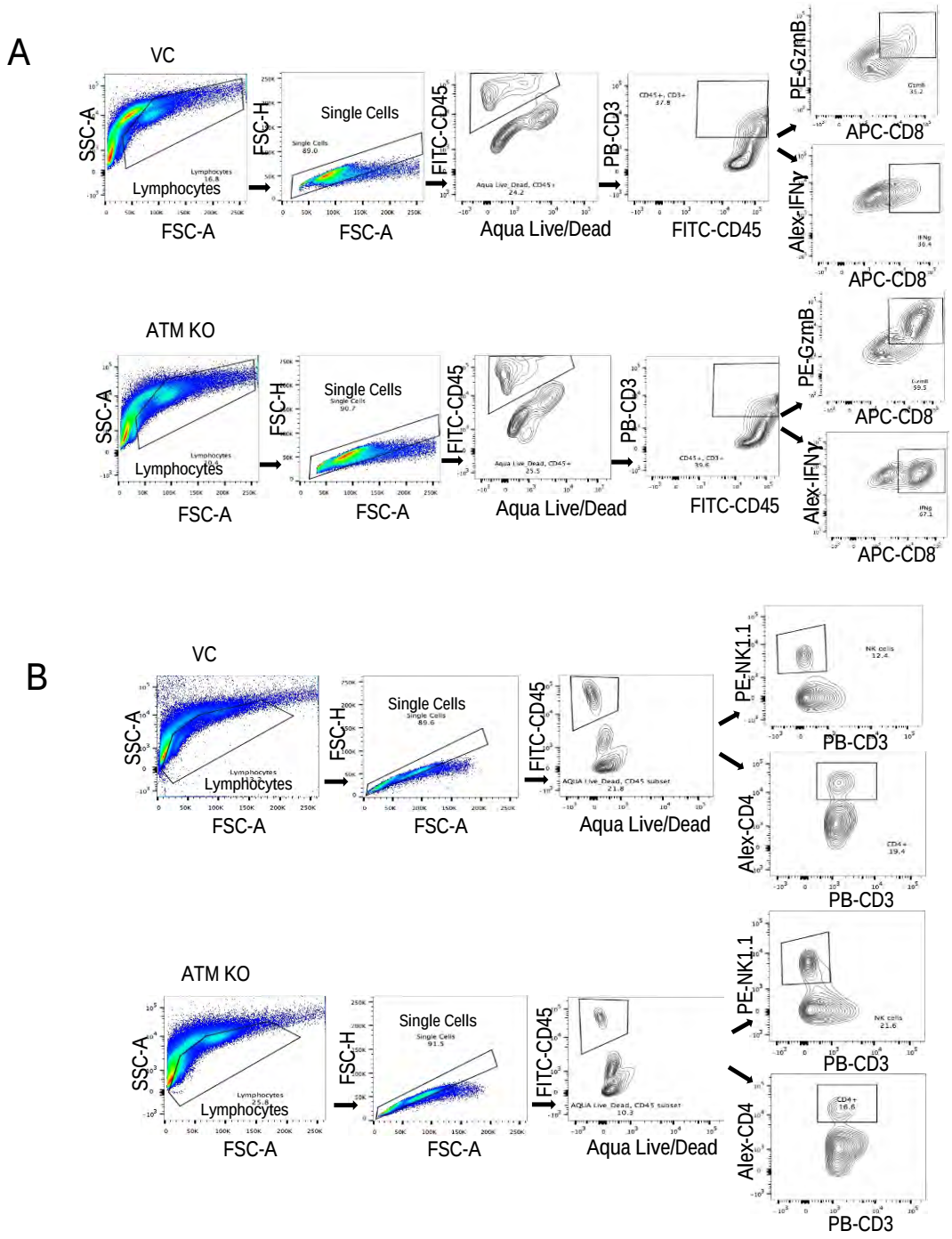

Supplementary Figure 11. Additional data on lymphocyte infiltration into ATM deficient tumors. (A) Gating strategy and representative flow cytometry plots for the quantification of $CD8^+$ T cells , $GzmB^+CD8^+$ and $IFN\gamma^+CD8^+$ T cells in vector control(VC) and ATM KO B16 tumors. (B) Gating strategy and representative flow cytometry graphs for the assessment of $CD4^+$ T cells and NK cells in vector control(VC) and ATM KO B16 tumors.

A

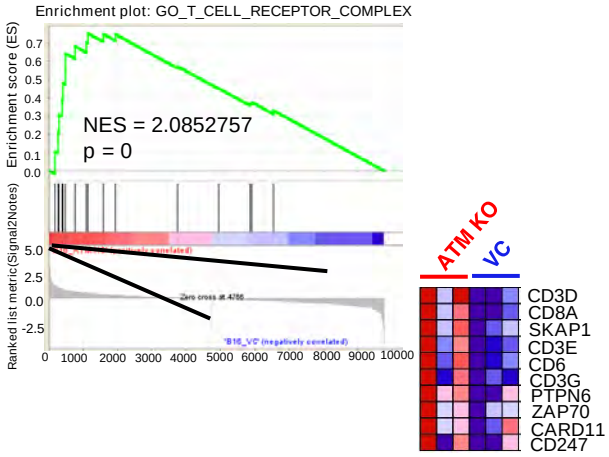

B

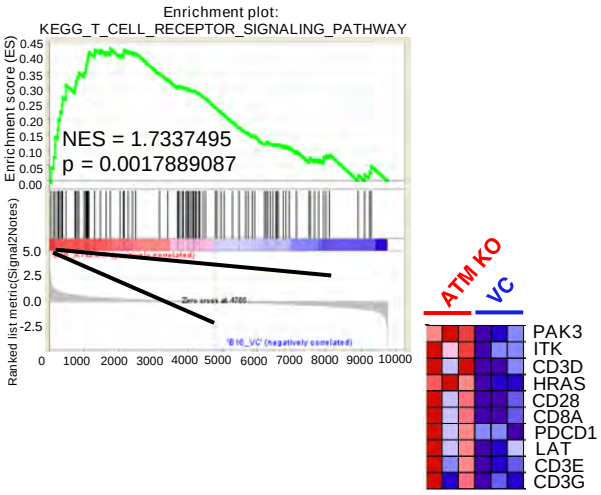

Supplementary Figure 12. RNAseq profiling of ATM deficient tumors in vivo. Gene set enrichment analysis (GSEA) of T cell receptor complex (A) and T cell receptor signaling (B) gene expression in control and B16F10 ATMKO tumors. FDR calculated using GSEA.

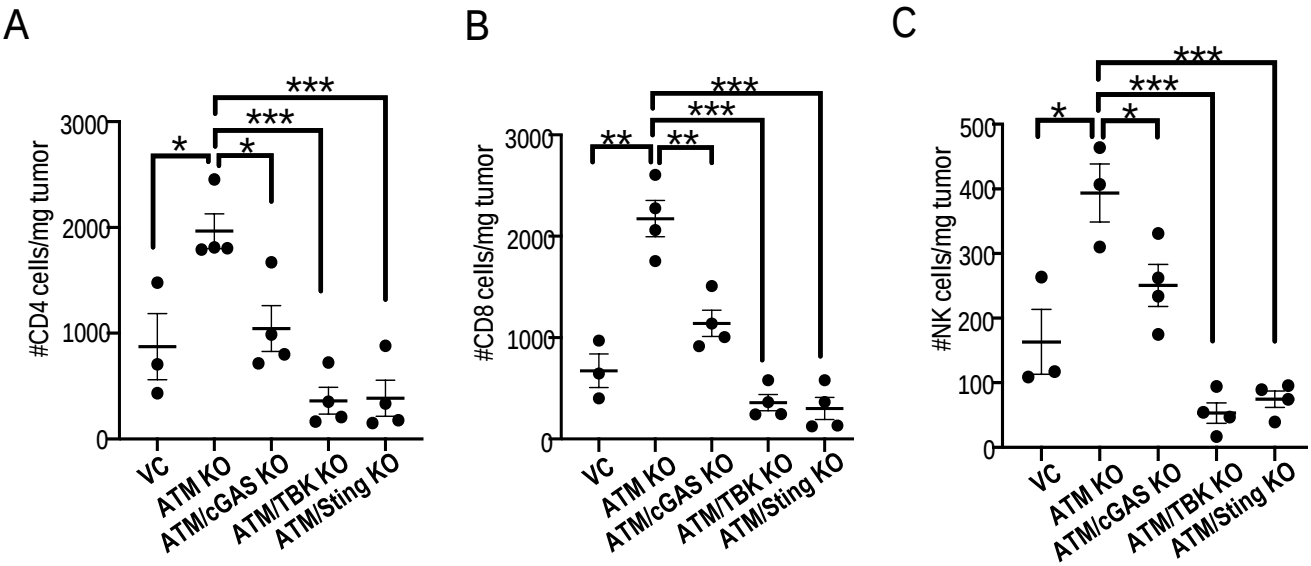

Supplementary Figure 13. Additional analysis of lymphocyte infiltration into ATM deficient tumors. Average numbers of tumor-infiltrating $CD4^+$ T cells (A), $CD8^+$ T cells (B), $NK1.1^+$ NK cells (C) in tumors established from vector control (VC) , ATM KO B16F10, ATM/cGas DKO, ATM/TBK DKO, ATM/STING DKO B16F10 tumor cells inoculated in C57BL/6 mice. Flow cytometry analysis were done on day 13 post inoculation of $1x10^5$ tumor cells. Error bars represent standard error of the mean (SEM). *p<0.05, **p<0.01, ***p<0.001, ****p<0.0001, ns, not significant, as determined by 2-way ANOVA

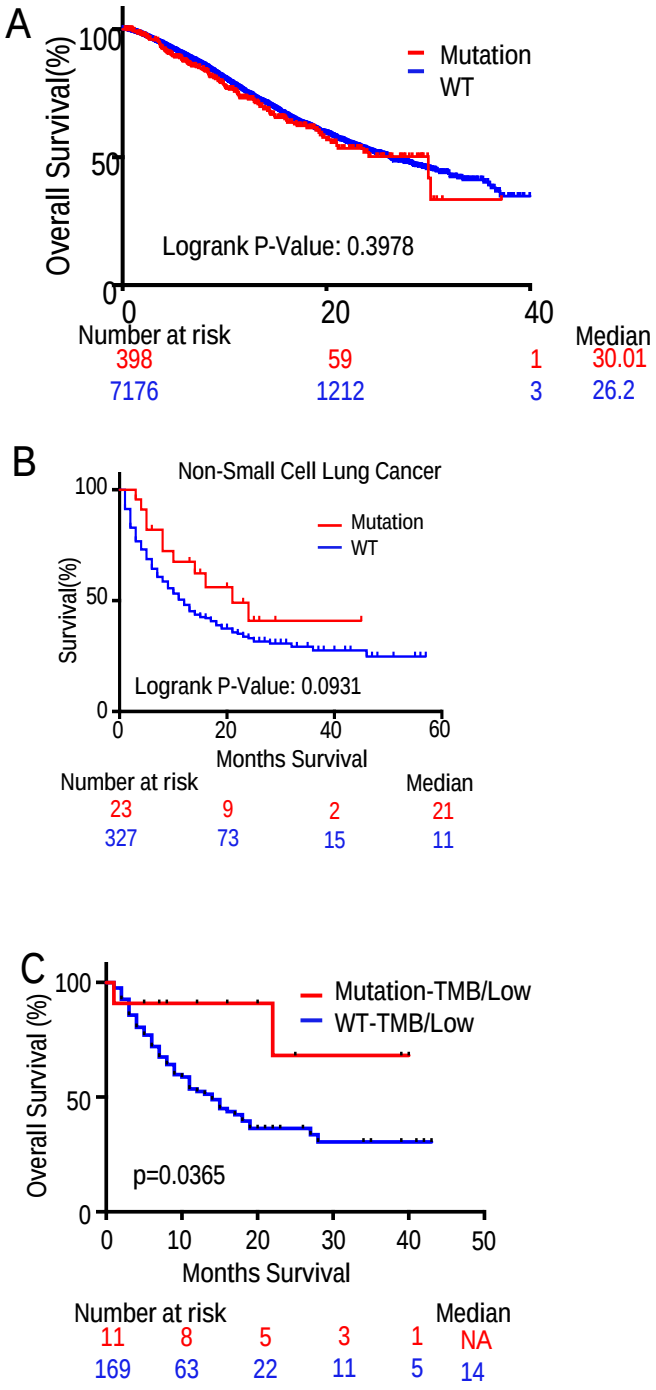

Supplementary Figure 14. Additional human clinical data regarding the influence of ATM mutations on tumor responses to ICB therapy. (A) Kaplan-Meier survival curve of patients from the whole MSK-IMPACT cohort with (red) or without (blue) ATM mutations who were not treated with ICB therapy. Data from the MSK-IMPACT clinical sequencing cohort (reference 43). (B) Kaplan-Meier survival data after immune checkpoint inhibitor therapy in non-small cell lung cancer patients with (red) or without (blue) ATM mutations. Data from the MSK-TMB cohort (reference 41). (C) Kaplan-Meier survival of curve of overall survival of patients with bladder cancer treated ICB therapy. Compared with Fig. 9D, only those patients with TMB<20 were considered to exclude the influence of MSI status. P values calculated by use of logrank test